HHS Public Access

Author manuscript

Nat Biotechnol. Author manuscript; available in PMC 2016 August 01.

Published in final edited form as:

Nat Biotechnol. 2016 March ; 34(3): 334–338. doi:10.1038/nbt.3469.

A dual AAV system enables the Cas9-mediated correction of a metabolic liver disease in newborn mice

Yang Yang[1,2,†], **Lili Wang**[3,*,†], **Peter Bell**[1], **Deirdre McMenamin**[1], **Zhenning He**[1], **John White**[1], **Hongwei Yu**[1], **Chenyu Xu**[4], **Hiroki Morizono**[4], **Kiran Musunuru**[5,6], **Mark L. Batshaw**[4], and **James M. Wilson**[1,*]

[1]Gene Therapy Program, Department of Medicine, Perelman School of Medicine, University of Pennsylvania, Philadelphia, PA, USA

[2]State Key Laboratory of Biotherapy and Cancer Center, West China Hospital, Sichuan University, and Collaborative Innovation Center for Biotherapy, Chengdu, Sichuan, China

[3]Gene Therapy Program, Department of Pathology and Laboratory Medicine, Perelman School of Medicine, University of Pennsylvania, Philadelphia, PA, USA

[4]Center for Genetic Medicine Research, Children's Research Institute, Children's National Health System, Washington, DC, USA

[5]Department of Stem Cell and Regenerative Biology, Harvard University, Harvard Stem Cell Institute, Cambridge, MA USA

[6]Division of Cardiovascular Medicine, Brigham and Women's Hospital, Boston, MA, USA

Abstract

Many genetic liver diseases present in newborns with repeated, often lethal, metabolic crises. Gene therapy using non-integrating viruses such as AAV is not optimal in this setting because the non-integrating genome is lost as developing hepatocytes proliferate[1,2]. We reasoned that newborn liver may be an ideal setting for AAV-mediated gene correction using CRISPR/Cas9. Here we intravenously infuse two AAVs, one expressing Cas9 and the other expressing a guide RNA and the donor DNA, into newborn mice with a partial deficiency in the urea cycle disorder enzyme, ornithine transcarbamylase (OTC). This resulted in reversion of the mutation in 10% (6.7% – 20.1%) of hepatocytes and increased survival in mice challenged with a high-protein diet, which

[*]Correspondence should be addressed to J.M.W. (; Email: wilsonjm@mail.med.upenn.edu): James M. Wilson, MD, PhD, Gene Therapy Program, Department of Medicine, University of Pennsylvania, Philadelphia, PA 19104, USA, Tel: 1-215-898-0226, Fax: 1-215-494-5444

[†]These authors contributed equally to this work.

Author Contributions

L.W. and J.M.W. conceived this study. L.W., Y.Y., and J.M.W. designed the experiments. Y.Y., P.B., D.M., Z.H., J.W., H.Y., and C.X. performed the experiments. K.M. conducted the bioinformatics analysis of the deep sequencing data. J.M.W., L.W., Y.Y., P.B., H.M., K.M., and M.L.B. wrote and edited the manuscript.

Competing Financial Interests

J.M. Wilson is an advisor to REGENXBIO, Dimension Therapeutics, Solid Gene Therapy, and Alexion, and is a founder of, holds equity in, and has a sponsored research agreement with REGENXBIO and Dimension Therapeutics; in addition, he is a consultant to several biopharmaceutical companies and is an inventor on patents licensed to various biopharmaceutical companies.

exacerbates disease. Gene correction in adult OTC-deficient mice was lower and accompanied by larger deletions that ablated residual expression from the endogenous *OTC* gene, leading to diminished protein tolerance and lethal hyperammonemia on a chow diet.

An X-linked deficiency of the OTC enzyme in humans causes recurrent and life-threatening episodes of hyperammonemia[3,4]. In males hemizygous for OTC deficiency, the first metabolic crisis usually occurs in the newborn period and is associated with up to 50% mortality, with survivors typically undergoing liver transplantation in the first year of life[5]. An animal model of OTC deficiency, the male sparse fur ash (*spf*^{ash}) mouse, has a G-to-A point mutation at the donor splice site at the end of exon 4 of the *OTC* gene, which leads to abnormal splicing and a 20-fold reduction in OTC mRNA and protein[6]. Affected animals have 5% residual OTC activity and can survive on a chow diet, but they develop hyperammonia that can be lethal when provided a high-protein diet.

In vivo genome editing of disease-causing mutations is a promising approach for the treatment of genetic disorders[7–17]. We developed a strategy using a dual-AAV system based on AAV8, which has high liver tropism to correct the point mutation in newborn *spf*^{ash} mice using Cas9 enzyme from *Staphylococcus aureus* (SaCas9)[11–13]. Prior to incorporating the individual components of the system into AAV8 vectors, we searched for protospacer-adjacent motif (PAM) sequences (NNGRRT) in proximity to the *spf*^{ash} mutation of the *OTC* gene and identified potential 20-nt protospacer sequences. Three sequences, sgRNA1–3 (Fig. 1a), were further evaluated following transfection of puromycin-containing plasmids into a mouse MC57G cell line. Evidence for double-strand breaks (DSBs) and the formation of indels at the desired site was demonstrated using the SURVEYOR assay (Supplementary Fig. 1a). One protospacer located within the adjacent intron (i.e., sgRNA3) failed to yield indels in this *in vitro* assay, while the others generated indels at the desired sites (Supplementary Fig. 1a). We selected the protospacer with a PAM within the adjacent intron (sgRNA1) because non-homologous end joining (NHEJ) without homology directed repair (HDR) within an exon could ablate residual OTC activity of the hypomorphic *spf*^{ash} mutation, thereby reducing residual ureagenesis. A plasmid cassette co-expressing the sgRNA1 guide RNA and SaCas9 was co-transfected with a plasmid containing a donor DNA template with approximately 0.9 kb of sequence flanking each side of the mutation. We mutated the corresponding PAM sequence in the donor template to reduce re-cleavage after HDR and included an *Age*I site facilitate detection of HDR, which was achieved with high-efficiency (Supplementary Fig. 1b).

A two-vector approach was necessary to incorporate all components into AAV (Fig. 1b). Vector 1 expressed the SaCas9 gene from a liver-specific TBG promoter (subsequently referred to as AAV8.SaCas9), while vector 2 contained the sgRNA1 sequence expressed from the U6 promoter and the 1.8 kb donor *OTC* DNA sequence (referred to as AAV8.sgRNA1.donor). In all experiments, *spf*^{ash} pups were injected intravenously on postnatal day 2 with mixtures of vector 1 and vector 2 and subsequently evaluated for indel formation and functional correction of the *spf*^{ash} mutation (Fig. 1c).

We obtained liver samples from treated *spf*^{ash} animals, untreated *spf*^{ash} (*spf*^{ash} controls), wildtype littermates, and *spf*^{ash} mice administered AAV8.SaCas9 with a modified

AAV8.control.donor without guide RNA (untargeted) at 1, 3, and 8 weeks following vector infusion. Pilot experiments elucidated optimal conditions of vector infusion with respect to doses and ratios of the two vectors (Supplementary Fig. 2). We administered 5×10^{11} genome copies (GC) of AAV8.sgRNA1.donor (or AAV8.control.donor) and 5×10^{10} GC of AAV8.SaCas9 in all newborn mouse experiments.

We analyzed the targeted region of the *OTC* gene by deep sequencing of PCR amplicons of liver tissue harvested 3 weeks (n=3) and 8 weeks (n=3) after vector treatment, and one untreated *spf*^{ash} mouse (Supplementary Table 1). More detailed descriptions of the actual indels from a subset of these animals is summarized in Supplementary Table 2. Following gene correction, indels were detected in 31% (26.5% – 35.5%) of *OTC* alleles from the 6 treated animals (Supplementary Table 1). More detailed studies in two treated mice indicated that over 90% of the deletions were less than 20 bp and only 1% extended into the adjacent exon (Supplementary Table 3). HDR-based correction of the G-to-A mutation was observed in 10% (6.7% – 20.1%) of *OTC* alleles from 6 treated animals (Supplementary Table 1). Analysis of amplified DNA between the G-to-A mutation and the donor-specific, altered PAM located 51 nt into the adjacent intron showed that approximately 83% of corrected alleles contained only donor derived-sequences between these two landmarks (reads with perfect HDR, Supplementary Table 1), while 3.5% of total *OTC* alleles had evidence of incomplete HDR events (reads with partial HDR, Supplementary Table 1). HDR-mediated targeted modifications were also estimated by the presence of a restriction-fragment length polymorphism (RFLP) introduced into the donor DNA in three animals harvested at each of the three time points. The average rate of HDR was 2.6% at 1 week, 18.5% at 3 weeks, and 14.3% at 8 weeks, confirming the high rate of HDR observed by deep sequencing (Supplementary Fig. 3a).

The algorithm described in www.benchling.com identified 49 potential off-target sites for sgRNA1. The top 16 sites most likely to create DSBs were amplified by PCR and deep sequenced (Supplementary Table 4). Samples from treated animals did not show indel rates above background (indel rates in untreated animals due to sequencing error, usually a fraction of a percent).

Tissue sections of liver were analyzed by immunohistochemistry for OTC expression. No signal (<1%) was observed in the *spf*^{ash} controls, while analysis of heterozygotes showed the predicted mosaicism (Fig. 2a). Morphometry indicated over 100-fold higher numbers of OTC-expressing cells in treated groups than found in the *spf*^{ash} control groups (Fig. 2b; 15% (6.8% – 24.4%) at 3 weeks and 13% (7.5% – 20.1%) at 8 weeks). Treated animals showed patches of OTC-expressing cells (Fig. 2c) that localized within all portions of the portal axis except around central veins, as predicted for endogenous OTC[18] Higher magnification showed clusters of OTC-expressing hepatocytes consistent with correction followed by clonal expansion in the context of the growing liver (Fig. 2d). Direct measurements of OTC enzyme activity from liver homogenates and OTC mRNA from total cellular liver RNA revealed similarly high levels of correction in treated animals, resulting in 20% (13.4% – 33.7%) and 16% (11.0% – 25.4%) of normal OTC enzyme activity at 3 and 8 weeks, respectively (Fig. 2e), and 13% (8.6% – 21.8%) and 9% (5.0% – 16.8%) of normal OTC mRNA at 3 and 8 weeks, respectively (Fig. 2f). Despite the decrease in OTC^{+} hepatocytes,

OTC enzyme activity, and OTC mRNA expression from 3 to 8 weeks, none of these differences were statistically significant (Fig. 2b; p=0.4828, Fig. 2e; p=0.2723, Fig. 2f; p=0.1475, respectively). OTC protein levels in liver of most treated animals were higher than in *spf*^{ash} controls but did not reach the levels found in wild-type mice (Supplementary Fig. 3b). Overall, there was good correlation of the estimates of correction based on histology, protein, and mRNA within individual animals.

One concern about using AAV to deliver SaCas9 is the virus's propensity to achieve stable transgene expression, which is not necessary to accomplish editing and may in fact contribute to immune and/or genome toxicity. Western blot analysis showed high level SaCas9 protein at 1 week that declined to undetectable levels by 8 weeks (Supplementary Fig. 3b). Furthermore, immunohistochemistry revealed nuclear-localized SaCas9 protein in 21% of hepatocytes at one week, which declined to undetectable levels (<0.1% hepatocytes) by 8 weeks (Fig. 3a). SaCas9 mRNA declined 43-fold during this 7-week period, to very low but still detectable levels (Fig. 3b). A 25-fold reduction in SaCas9 DNA during this same time interval indicates that elimination of vector genomes in the setting of the proliferating newborn liver is a primary contributor to the desired decline of SaCas9 expression (Fig. 3c). SaCas9 mRNA/vector copy did not change over time, indicating that the TBG promoter was still active.

In assessing the impact of gene correction on the clinical manifestations of OTC deficiency, we evaluated the tolerance of *spf*^{ash} mice to a one-week course of a high-protein diet and found that blood ammonia was elevated from 83 ± 9 μM (n=13) in wild type controls to 312 ± 30 μM (n=16) in the *spf*^{ash} controls at the end of the diet course (Fig. 3d; p<0.0001). Substantial variation in blood ammonia levels was found in untreated *spf*^{ash} animals after the one-week diet course, which is consistent with findings in OTC-deficient patients, who show large fluctuations in ammonia over relatively short periods of time[3]. There was no significant difference between untreated *spf*^{ash} and untargeted *spf*^{ash} controls (Fig. 3d; p=0.83). In contrast, we observed a statistically significant 40% reduction in ammonia in treated as compared to untreated *spf*^{ash} animals (Fig. 3d; p=0.0014), and treated *spf*^{ash} mice showed a survival improvement (Fig. 3e; p=0.03). During the course of the high-protein diet, 30% of both untreated *spf*^{ash} (n=20) and untargeted *spf*^{ash} animals (n=13) developed clinical signs of hyperammonemia and died or had to be euthanized, while all of the wild type mice (n=13) and treated *spf*^{ash} mice (n=13) survived (Fig. 3e). Detailed histological analyses of liver and transaminase levels (both alanine and aspartate aminotransferase, ALT and AST, respectively) in SaCas9-treated *spf*^{ash} mice harvested at the end of the high-protein diet challenge failed to reveal any pathology or toxicity (Supplementary Fig. 4).

Based on encouraging results in newborn *spf*^{ash} mice, we then conducted similar studies in adult *spf*^{ash} mice, which were infused with two different doses of the AAV vectors and euthanized 2 to 3 weeks later. Sequence analysis of on-target DNA amplicons revealed remarkably high frequencies of indels at both low and high vector doses (**Table 1**; 44.6% (38.5% – 50.3%) and 42.0% (34.0% – 48.5%), respectively) but low levels of gene correction as measured by reversion of the G-to-A mutation (**Table 1**; 0.3% (0.2% – 0.3%) and 1.7% (1.3% – 2.1%), respectively). Additional evidence of correction was provided by immunofluorescence analysis of liver for OTC expression that showed 2.2% (0.71%, 2.51%,

3.45%) and 6.0% (3.11%, 5.05%, 9.86%) positive cells in low- and high-dose animals, respectively (Fig. 4a; n=3 per group). Adults showed a pattern of isolated OTC-positive cells (Fig. 4b), while clusters of OTC-positive cells were present in newborns (Fig. 3c). Between 3 to 4 weeks after treatment with low-dose vectors, the animals unexpectedly became sick and by week 5 all had to be euthanized (Fig. 4c). This toxicity was more severe in the high-dose animals, requiring termination of the study at 2 weeks (Fig. 4d). Further analysis of symptomatic animals demonstrated dose-dependent elevations of urine orotate (Fig. 4e) and plasma ammonia (Fig. 4f) on a chow diet. These findings suggested a compromise of residual ureagenesis that could not be explained by liver damage since liver histology appeared normal (Supplementary Fig. 5a) and serum transaminases were slightly, but not statistically, elevated over control groups (Supplementary Fig. 5b). Deep sequencing of the targeted region of the *OTC* gene revealed a surprising number of large deletions in adults as compared to what was observed in newborns, with 6.5% extending into the adjacent exon in adults as opposed to 1% in newborns (Supplementary Table 3). The more complex and extensive indels in adult *spf*^{ash} mice were unlikely to have been caused by higher and/or more persistent Cas9 expression since Cas9 mRNA was lower in 3-week adults (Fig. 4g) than in any liver tissues harvested up to 8 weeks after injection in newborns (Supplementary Fig. 6a and b). We speculate that different NHEJ mechanisms may exist in non-dividing adult hepatocytes versus dividing newborn hepatocytes that affects the quality of the DNA repair response.

A key challenge in using the CRISPR/Cas9 system to correct a mutation *in vivo* is delivering the three components of the system (sgRNA, Cas9, and donor DNA) into the same cell in a way that is safe and efficient[19,20]. One recent report in the literature approached a similar challenge by utilizing chemically modified mRNA to deliver therapeutic levels of another site-specific endonuclease into murine lung[21]. Here, we leveraged our experience with liver-directed gene replacement therapy with highly hepatotropic AAV vectors[22] to move closer to realizing these goals in a model of liver metabolic disease. While the focus on newborn animals was driven by a compelling unmet need in patients with these lethal metabolic diseases, it also created some unique technical advantages. The surprisingly high level of correction in our newborn experiments is likely due to high expression of SaCas9 with abundant donor DNA in the context of dividing cells. Our previous studies of AAV8 gene transfer in newborn monkeys demonstrated the same high peak levels of transduction and gene transfer (i.e., 92% hepatocytes expressing GFP and 32 vector genomes per cell) as achieved in mice administered the same dose of GFP-expressing vector (i.e., 80% hepatocytes expressing GFP and 14 vector genomes per cell) with similar kinetics of decline, which is encouraging in terms of translation to larger species including humans[2,23].

Issues of safety relate primarily to the expression of Cas9 in the context of an sgRNA that could create off-target DSBs with carcinogenic sequelae, although our findings in the adult mice suggest that large on-target deletions could potentially be a safety issue in some contexts. More extensive characterization of these potential toxicities is necessary before clinical translation can be considered[24,25], although, in animals treated as newborns, we could not detect indels of likely off-target sites at the level of sensitivity achieved by deep sequencing. Cas9 could also elicit pathologic immune responses[16], as has been observed in gene replacement therapies in which the transgene is a foreign protein. However, systemic

delivery of AAV in a newborn helps mitigate potential immunologic adverse events for several reasons[26–28]. First, expression of the prokaryotic SaCas9 protein is transient because the non-integrated vector is lost during hepatocyte proliferation[1]. Furthermore, we have shown that exposure of newborn rhesus macaques to AAV-encoded proteins induces tolerance to these proteins, thereby circumventing toxicity caused by destructive adaptive immune responses[29].

This study provides convincing evidence for efficacy in an authentic animal model of a lethal human metabolic disease following *in vivo* genome editing. Furthermore, our observation of dramatic differences in clinical outcome following HDR-mediated gene correction of newborn versus adult animals illustrates potential unintended consequences of NHEJ-mediated ablation of residual function in hypomorphic mutant genes that may complicate some applications of therapeutic genome editing.

Online Methods

Plasmid construction

The smaller-sized Cas9 from *Staphylococcus aureus* (SaCas9) is more suitable for packaging into an AAV vector. We codon-optimized FLAG-tagged SaCas9 according to human codon usage (hSaCas9) and constructed pX330.hSaCas9 by replacing the hSpCas9 and sgRNA scaffold in pX330 with hSaCas9 and SaCas9 sgRNA scaffold. Three 20-nt target sequences preceding a 5′NNGRRT PAM sequence were selected for *OTC* gene editing. A puromycin-resistance gene cassette was cloned into pX330.hSaCas9-derived plasmids for selection of transfected cells following *in vitro* transient transfection. To generate a dual AAV vector system for *in vivo OTC* gene correction by SaCas9, we constructed two AAV cis-plasmids: 1) the hSaCas9 was subcloned from pX330.hSaCas9 into an AAV backbone plasmid containing the full-length TBG promoter (two copies of enhancer elements of the α microglobulin/bikunin gene followed by a liver-specific TBG promoter) and the bovine growth hormone polyadenylation sequence, yielding AAV8.SaCas9; 2) the 1.8-kb *OTC* donor template was cloned into the pAAV backbone, and the U6-*OTC* sgRNA1 cassette was inserted into the *Afl*II site, yielding AAV8.sgRNA1.donor. The PAM sequence in the donor template in AAV8.sgRNA1.donor was mutated to prevent re-cleavage by Cas9 after HDR, and an *Age*I site was added to facilitate detection of HDR (Supplementary Table 5). The “untargeted” AAV8.control.donor differs from the “targeted” AAV8.sgRNA1.donor by eliminating the protospacer from the U6-OTC sgRNA1 cassette. All plasmid constructs were verified by sequencing.

AAV vector production

All AAV8 vectors were produced by the Penn Vector Core at the University of Pennsylvania as previously described[30]. The genome titer (GC mL^{-1}) of AAV vectors was determined by quantitative PCR (qPCR). All vectors used in this study passed the endotoxin assay using the QCL-1000 Chromogenic LAL test kit (Cambrex Bio Science).

Cell culture and transfection

MC57G cells (ATCC) were maintained in DMEM medium supplemented with 10% FBS and cultured at 37°C with 5% CO_2. Cell lines were used directly upon receipt from ATCC and were not authenticated or tested for mycoplasma contamination. For *in vitro* target and/or donor template testing, plasmids were transfected into MC57G cells using Lipofectamine® LTX with Plus™ reagent (Life Technology) per manufacturer's recommendations. Transfected cells were under puromycin (4 μg mL^{-1}) selection for 4 days to enrich transfected cells.

Genomic DNA extraction and SURVEYOR assay

Genomic DNA from transfected MC57G cells was extracted using the QuickExtract DNA extraction solution (Epicentre Biotechnologies). The efficiency of each individual sgRNA was tested by the SURVEYOR nuclease assay (Transgenomics) as described previously[31] using the PCR primers listed in Supplementary Table 5.

Animal studies

spf^{ash} mice were maintained in an AAALAC (Association for Assessment and Accreditation of Laboratory Animal Care)-accredited and PHS (Public Health Service)-assured facility at the University of Pennsylvania, as described previously[32]. All animal procedures were performed in accordance with protocols approved by the Institutional Animal Care and Use Committee (IACUC) of the University of Pennsylvania. Mating cages were monitored daily for births. Newborn (postnatal day 2, p2) male pups received a temporal vein injection of the mixture of two vectors at the intended doses for each in a volume of 50 μl, as described[33]. Untreated wild-type (WT), *spf*^{ash} heterozygous (Het), and *spf*^{ash} hemizygous mice served as controls. Mice were sacrificed at 1, 3, or 8 weeks after vector treatment, and liver samples were harvested for analyses. Mice were genotyped at weaning or at the time of necropsy to confirm genotype.

For testing the efficacy of *OTC* correction, a high-protein diet (40% protein, Animal Specialties & Provisions) was given to 7-week-old mice for 7 days. After this time, plasma was collected for measurement of plasma NH_3 using the Sigma Ammonia Assay Kit. The remaining samples were sent to Antech Diagnostics for measurements of ALT, AST, and total bilirubin.

Note that the entire litter of newborn male pups was injected with either the test or control vectors, and no specific randomization method was used. The following assays were performed in a blinded fashion in which the investigator was unaware of the nature of the vectors or vector dose: vector injection, OTC and Cas9 (FLAG) immunostaining and quantification, histopathology analysis on liver, OTC enzyme activity assay, and gene expression analysis and RT-qPCR.

The adult gene editing experiments were conducted in 8- to 10-week-old male *spf*^{ash} mice. Animals in low-dose groups received a tail vein injection of AAV8.SaCas9 (1×10^{11}GC) and AAV8.sgRNA1.donor (1×10^{12} GC) or untargeted vectors at the same doses, and they were sacrificed at 3 weeks after injection for analyses. Animals in high-dose groups received a tail

vein injection of AAV8.SaCas9 (1×10^{12} GC) and AAV8.sgRNA1.donor (5×10^{12} GC) or untargeted vectors at the same doses, and they were sacrificed at 2 weeks after injection for analyses.

OTC and Cas9 immunostaining

Immunofluorescence for OTC expression was performed on frozen liver sections. Cryosections (8 μm) were air dried and fixed in 4% paraformaldehyde (all solutions in phosphate-buffered saline) for 10 min. Sections were then permeabilized and blocked in 0.2% Triton containing 1% donkey serum for 30 min. A rabbit anti-OTC antibody[34] (diluted 1:1000 in 1% donkey serum) was used to incubate the sections for 1 hr. After washing, the sections were stained with tetramethylrhodamine (TRITC)–conjugated donkey anti-rabbit antibodies (Jackson Immunoresearch Laboratories, Cat# 711–025–152) in 1% donkey serum for 30 min, washed, and mounted with Vectashield (Vector Laboratories).

Some sections were additionally stained with a monoclonal antibody against glutamine synthetase (BD Biosciences, clone 6, Cat# 610517) as a marker for pericentral hepatocytes followed by fluorescein isothiocyanate (FITC)-labeled donkey anti-mouse antibodies (Jackson Immunoresearch Laboratories, Cat# 715–095–150). Double staining was performed by mixing the two primary and secondary antibodies, respectively, and following the above protocol. Other sections were counterstained with fluorescein-labeled tomato lectin (Lycopersicon esculentum lectin, LEL; Vector Laboratories, Cat# FL-1171) by adding LEL to the secondary antibody solution at a dilution of 1:500.

Cas9 expression was detected on sections from paraffin-embedded livers via immunostaining for FLAG tag using monoclonal antibody M2 (Sigma, Cat# F1804). Paraffin sections were processed according to standard protocols with an antigen retrieval step (boiling for 6 min in 10 mM citrate buffer, pH 6.0). Staining was performed using a mouse-on-mouse (MOM) kit (Vector Laboratories) according to the manufacturer's instructions.

To quantify percentages of OTC-expressing hepatocytes, 10 random images were taken with a 10x objective from each liver section stained for OTC expression. In some cases, where only a small liver section was available, only 5 pictures were taken. Using ImageJ software (Rasband W. S., National Institutes of Health, USA; http://rsb.info.nih.gov/ij/), images were thresholded for OTC-positive area (i.e. the OTC-positive area was selected) and the percentage of the OTC-positive area was determined for each image. In a second measurement the images were thresholded for "empty" area (e.g., veins and sinusoids) to determine the percentage of the area not occupied by liver tissue. This was possible as a result of the presence of weak background fluorescence of the liver tissue. The final percentage of OTC-positive liver tissue (i.e., OTC-positive hepatocytes) was then calculated per adjusted area (total area minus empty area), and the values were averaged for each liver.

To determine the percentage of Cas9-positive hepatocytes, two sections from each liver were analyzed, one stained for Cas9 (via FLAG tag), the other section stained with hematoxylin to label all nuclei. Three images from every section were taken with a 10x objective, and the number of either Cas9-positive or hematoxylin-stained hepatocyte nuclei was determined

using ImageJ's "Analyze Particles" tool that allows one to select and count stained hepatocyte nuclei. Hematoxylin-stained nuclei from other cell types could be excluded based on size and circularity parameters. The percentage of Cas9-positive nuclei was then calculated based on the total number of hepatocyte nuclei visible in the hematoxylin-stained sections.

Histopathology

Hematoxylin and eosin (H&E) staining was performed on sections from paraffin-embedded liver samples processed and stained according to standard protocols. Sections were analyzed for any abnormalities compared to livers from untreated animals.

OTC enzyme activity assay

OTC enzyme activity was assayed in liver lysates as described previously with modifications[35]. Whole-liver fragments were frozen in liquid nitrogen and stored at −80°C until OTC measurements were performed. A homogenate of 50 mg liver tissue per mL was prepared in 50 mM Tris acetate buffer, pH 7.5, with a Polytron homogenizer (Kinematica AG). A total of 250 μg of liver tissue was used per assay tube, and assays were performed in duplicate. The protein concentration was determined on the remaining liver homogenate using the Bio-Rad Protein assay kit (Bio-Rad) according to the manufacturer's instructions.

Western blot analysis

Western blot analyses were performed on liver lysates as described previously[36]. OTC protein was detected by a custom rabbit polyclonal antibody (1:10,000 dilution)[34]. Mouse anti-FLAG M2 antibody (1:2000 dilution, Sigma, Cat# F1804) and mouse anti-actin antibody (1:1,000 dilution, Cell Signaling Technology, Cat# 8457L) were used to detect Cas9 and actin. Blots were imaged with ChemiDoc MP system and analyzed using ImageLab 4.1 software (Bio-Rad).

Gene expression analysis and RT-qPCR

RNA was isolated using Trizol (Life Technology) and reverse-transcribed using a High-Capacity cDNA Reverse Transcription Kit (Applied Biosystems). qPCR to measure murine OTC, SaCas9, and GAPDH were performed using gene-specific primers (Life Technologies). Data were normalized to GAPDH levels.

On-target and off-target mutagenesis analyses

HDR-mediated targeted modifications were confirmed by restriction-fragment length polymorphism (RFLP) analysis, as described previously[31]. The HDR-Fwd and HDR-Rev primers were designed to anneal outside of the region of homology between the donor template and targeted genomic region. The PCR products were purified and digested with *Age*I restriction enzyme. To further analyze the *OTC* intron 4 on-target site, the genomic region was amplified by nested PCR. Briefly, the genomic DNA was first amplified by the HDR-Fwd and HDR-Rev primers (Supplementary Table 5) using Q5® High-Fidelity DNA Polymerase (New England Biolabs) and gel purified to remove the residual AAV8.sgRNA1.donor in the genomic DNA. Then nested PCR was performed by using the

purified 1st round PCR amplicon. Libraries were made from 250 ng of the 2nd PCR products using NEBNext® Ultra™ DNA Library Prep Kit for Illumina (NEB) and sequenced on Illumina MiSeq (2×250 base pair (bp) paired end or 2×300 bp paired end, Genewiz). Data were processed according to standard Illumina sequencing analysis procedures. Processed reads were mapped to the expected PCR amplicons as reference sequences using custom scripts. Reads that did not map to reference were discarded. Insertions and/or deletions were determined by comparison of reads against reference using custom scripts. The indel sequences as summarized for the *OTC* intron 4 on-target site are presented in Supplementary Table 2.

The most likely off-target sites were determined using the algorithm described in www.benchling.com, referred to as OT1 through OT16 (Supplementary Table 4). Primers spanning these sites (Supplementary Table 6) were used to amplify relevant sequences by nested PCR. Purified PCR fragments were then subjected to deep sequencing as described above.

Frequencies of on-target and off-target indels and on-target correction of the *spf*^{ash} mutation were determined as follows. MiSeq reads were analyzed using custom scripts to identify indels by matching reads against reference, with indels involving any portion of the sequence within 15 nt upstream or downstream of the predicted CRISPR-Cas9 cleavage site (3 nt downstream of the PAM, within the protospacer) considered to be possible off-target effects. Reads for which there was any 18-nt sequence with more than 2 mismatches with the corresponding 18-nt portion of the reference sequence, either upstream or downstream of a candidate indel, were discarded as errors. All candidate indels for the OT1 through OT16 sites were manually curated for confirmation.

For the *OTC* intron 4 on-target site, a read was counted as having “Perfect HDR” if on the antisense strand there was a perfect match with a 51-nt sequence from the donor, starting with the donor-specific ‘CACCAA’ at the location of the PAM, through the donor-specific *Age*I insert ‘ACCGGT’, and ending with the SNV ‘C’ at the *spf*^{ash} *OTC* mutation site. A read was counted as being a “Read with a ‘G’” if it either (1) met the criterion for “Perfect HDR” or (2) had the SNV ‘G’ on the sense strand in the expected *spf*^{ash} *OTC* mutation site 54 nt upstream of the predicted CRISPR-Cas9 cleavage site (accounting for the size of the donor-specific *Age*I insert ‘ACCGGT’), with up to two mismatches with the 18-nt intronic portion of the reference sequence adjacent to the *spf*^{ash} *OTC* mutation site. A read was counted as having “Partial HDR” if it did not meet the criteria for “Perfect HDR” and “Read with a ‘G’” and if there was a perfect match with an 18-nt sequence from the donor, starting with the donor-specific ‘CACCAA’ at the 3′ end of the target site and ending with the donor-specific *Age*I insert ‘ACCGGT’.

Statistical analyses

Test and control vectors were evaluated in at least 3 mice per group at each time point to ensure reproducibility. Sample sizes are noted in figure legends. All animals with successful temporal vein injection were included in the study analysis. Those animals with unsuccessful injection were excluded. Injection success was determined according to vector

genome copies in liver via qPCR, where animals with vector genome copies <10% of the mean value of the dosing group at the same time point were considered to be unsuccessful.

Statistical analyses were performed with GraphPad Prism 6.03 for Windows. The Dunnett's multiple comparisons test was used to compare a number of variables with a single control. Due to the relatively small sample size, normality testing was not feasible. The Mantel-Cox test was used to test the survival distributions for differences. Group averages are presented as mean ± S.E.M.

Supplementary Material

Refer to Web version on PubMed Central for supplementary material.

Acknowledgments

We thank Penn Vector Core for supplying vectors, Penn Bioinformatics Core for assistance on deep sequencing data analysis, Y. Zhu and M. Nayalat for help on immunohistochemistry analysis, and L. Mays for assistance on manuscript preparation. This work was supported by NICHD P01-HD057247 (J.M.W.) and the Kettering Family Foundation (M.B.).

References

1. Cunningham SC, Dane AP, Spinoulas A, Logan GJ, Alexander IE. Gene delivery to the juvenile mouse liver using AAV2/8 vectors. Mol Ther. 2008; 16:1081–1088. [PubMed: 18414478]
2. Wang L, Wang H, Bell P, McMenamin D, Wilson JM. Hepatic gene transfer in neonatal mice by adeno-associated virus serotype 8 vector. Hum Gene Ther. 2012; 23:533–539. [PubMed: 22098408]
3. Batshaw ML, Tuchman M, Summar M, Seminara J. A longitudinal study of urea cycle disorders. Mol Genet Metab. 2014; 113:127–130. [PubMed: 25135652]
4. Lichter-Konecki, U.; Caldovic, L.; Morizono, H.; Simpson, K. Pagon, RA.; Adam, MP.; Ardinger, HH., et al., editors. Ornithine Transcarbamylase Deficiency (1993–2013). GeneReviews®. (http://www.ncbi.nlm.nih.gov/books/NBK154378/)
5. Ah Mew N, Krivitzky L, McCarter R, Batshaw M, Tuchman M. Clinical outcomes of neonatal onset proximal versus distal urea cycle disorders do not differ. J Pediatr. 2013; 162:324–329. e321. [PubMed: 22901741]
6. Hodges PE, Rosenberg LE. The spfash mouse: a missense mutation in the ornithine transcarbamylase gene also causes aberrant mRNA splicing. Proc Natl Acad Sci U S A. 1989; 86:4142–4146. [PubMed: 2471197]
7. Sharma R, et al. In vivo genome editing of the albumin locus as a platform for protein replacement therapy. Blood. Epub ahead of print.
8. Yin H, et al. Genome editing with Cas9 in adult mice corrects a disease mutation and phenotype. Nat Biotechnol. 2014; 32:551–553. [PubMed: 24681508]
9. Anguela XM, et al. Robust ZFN-mediated genome editing in adult hemophilic mice. Blood. 2013; 122:3283–3287. [PubMed: 24085764]
10. Barzel A, et al. Promoterless gene targeting without nucleases ameliorates haemophilia B in mice. Nature. 2015; 517:360–364. [PubMed: 25363772]
11. Ran FA, et al. In vivo genome editing using Staphylococcus aureus Cas9. Nature. 2015; 520:186–191. [PubMed: 25830891]
12. Friedland AE, et al. Characterization of Staphylococcus aureus Cas9: a smaller Cas9 for all-in-one adeno-associated virus delivery and paired nickase applications. Genome Biol. 2015; 16:257. [PubMed: 26596280]
13. Kleinstiver BP, et al. Engineered CRISPR-Cas9 nucleases with altered PAM specificities. Nature. 2015; 523:481–485. [PubMed: 26098369]

14. Hsu PD, Lander ES, Zhang F. Development and applications of CRISPR-Cas9 for genome engineering. Cell. 2014; 157:1262–1278. [PubMed: 24906146]
15. Doudna JA, Charpentier E. Genome editing. The new frontier of genome engineering with CRISPR-Cas9. Science. 2014; 346:1258096. [PubMed: 25430774]
16. Wang D, et al. Adenovirus-mediated somatic genome editing of Pten by CRISPR/Cas9 in mouse liver in spite of Cas9-specific immune responses. Hum Gene Ther. 2015; 26:432–442. [PubMed: 26086867]
17. Cheng R, et al. Efficient gene editing in adult mouse livers via adenoviral delivery of CRISPR/Cas9. FEBS Lett. 2014; 588:3954–3958. [PubMed: 25241167]
18. Dingemanse MA, et al. Development of the ornithine cycle in rat liver: zonation of a metabolic pathway. Hepatology. 1996; 24:407–411. [PubMed: 8690412]
19. Schmidt F, Grimm D. CRISPR genome engineering and viral gene delivery: a case of mutual attraction. Biotechnol J. 2015; 10:258–272. [PubMed: 25663455]
20. Vasileva A, Jessberger R. Precise hit: adeno-associated virus in gene targeting. Nat Rev Microbiol. 2005; 3:837–847. [PubMed: 16261169]
21. Mahiny AJ, et al. In vivo genome editing using nuclease-encoding mRNA corrects SP-B deficiency. Nat Biotechnol. 2015; 33:584–586. [PubMed: 25985262]
22. Gao GP, et al. Novel adeno-associated viruses from rhesus monkeys as vectors for human gene therapy. Proc Natl Acad Sci U S A. 2002; 99:11854–11859. [PubMed: 12192090]
23. Wang L, et al. AAV8-mediated hepatic gene transfer in infant rhesus monkeys (Macaca mulatta). Mol Ther. 2011; 19:2012–2020. [PubMed: 21811248]
24. Yang L, et al. Targeted and genome-wide sequencing reveal single nucleotide variations impacting specificity of Cas9 in human stem cells. Nat Commun. 2014; 26:5507. [PubMed: 25425480]
25. Tsai SQ, et al. GUIDE-seq enables genome-wide profiling of off-target cleavage by CRISPR-Cas nucleases. Nat Biotechnol. 2015; 33:187–97. [PubMed: 25513782]
26. Shi Y, Falahati R, Zhang J, Flebbe-Rehwaldt L, Gaensler KM. Role of antigen-specific regulatory CD4+CD25+ T cells in tolerance induction after neonatal IP administration of AAV-hF.IX. Gene Ther. 2013; 20:987–996. [PubMed: 23759700]
27. Nivsarkar MS, et al. Evidence for contribution of CD4+ CD25+ regulatory T cells in maintaining immune tolerance to human factor IX following perinatal adenovirus vector delivery. J Immunol Res. 2015; 2015
28. LoDuca PA, Hoffman BE, Herzog RW. Hepatic gene transfer as a means of tolerance induction to transgene products. Curr Gene Ther. 2009; 9:104–114. [PubMed: 19355868]
29. Hinderer C, et al. Neonatal Systemic AAV Induces Tolerance to CNS Gene Therapy in MPS I Dogs and Nonhuman Primates. Mol Ther. 2015; 23:1298–1307. [PubMed: 26022732]
30. Lock M, et al. Rapid, simple, and versatile manufacturing of recombinant adeno-associated viral vectors at scale. Hum Gene Ther. 2010; 21:1259–1271. [PubMed: 20497038]
31. Ran FA, et al. Genome engineering using the CRISPR-Cas9 system. Nat Protoc. 2013; 8:2281–2308. [PubMed: 24157548]
32. Moscioni D, et al. Long-term correction of ammonia metabolism and prolonged survival in ornithine transcarbamylase-deficient mice following liver-directed treatment with adeno-associated viral vectors. Mol Ther. 2006; 14:25–33. [PubMed: 16677864]
33. Daly TM. AAV-mediated gene transfer to the liver. Methods Mol Biol. 2004; 246:195–199. [PubMed: 14970593]
34. Augustin L, Mavinakere M, Morizono H, Tuchman M. Expression of wild-type and mutant human ornithine transcarbamylase genes in Chinese hamster ovary cells and lack of dominant negative effect of R141Q and R40H mutants. Pediatr Res. 2000; 48:842–846. [PubMed: 11102556]
35. Morizono H, et al. Expression, purification and kinetic characterization of wild-type human ornithine transcarbamylase and a recurrent mutant that produces ‘late onset’ hyperammonaemia. Biochem J. 1997; 322(Pt 2):625–631. [PubMed: 9065786]
36. Wang L, et al. Sustained correction of OTC deficiency in spf(ash) mice using optimized self-complementary AAV2/8 vectors. Gene Ther. 2012; 19:404–410. [PubMed: 21850052]

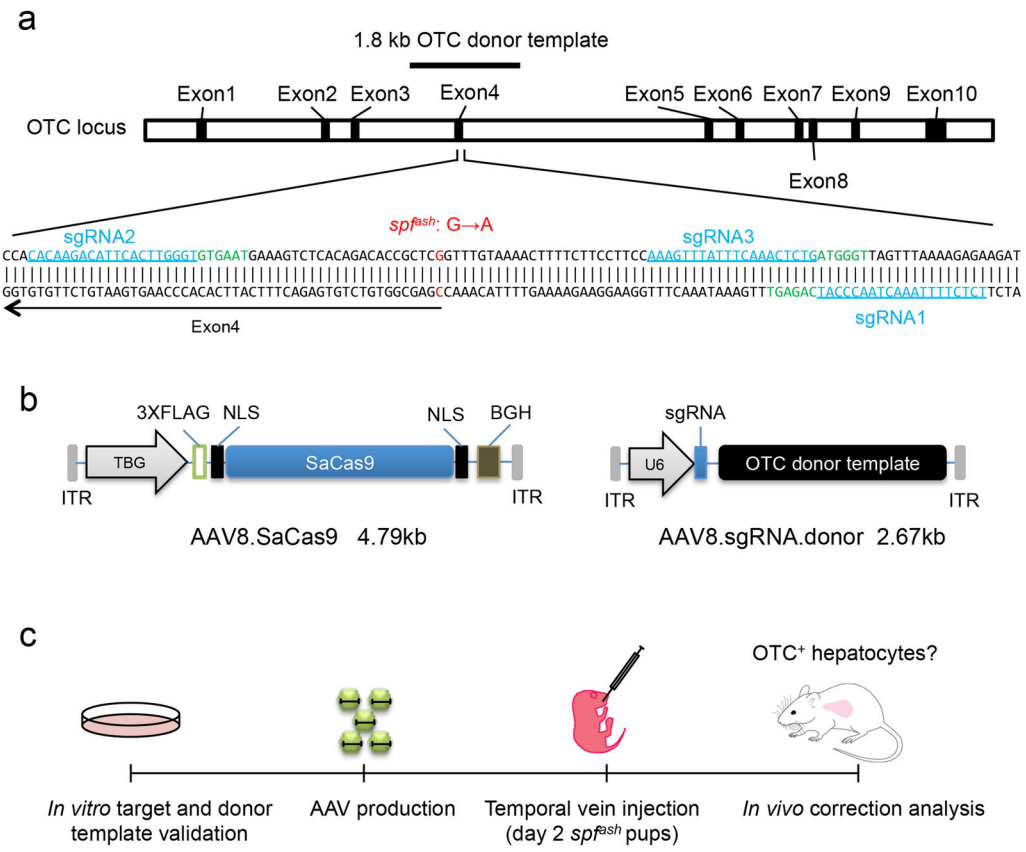

Figure 1. *In vivo* gene correction of the *OTC* locus in the *spf*^{ash} mouse liver by AAV.CRISPR-SaCas9

(**a**) Schematic diagram of the mouse *OTC* locus showing the *spf*^{ash} mutation and three SaCas9 targets. *spf*^{ash} has a G-to-A mutation at the donor splice site at the end of exon 4 indicated in red on the top strand. The three selected SaCas9-targeted genomic sites (20 bp each) are in blue and underlined with the PAM sequences marked in green. The black line above exon 4 indicates the 1.8 kb *OTC* donor template. (**b**) Dual AAV vector system for liver-directed and SaCas9-mediated gene correction. The AAV8.sgRNA1.donor vector contains a 1.8-kb murine *OTC* donor template sequence as shown in (**a**) with the corresponding PAM sequence mutated and an *Age*I site inserted. (**c**) Flowchart showing the key steps of AAV8.CRISPR-SaCas9-mediated gene correction in the neonatal *OTC spf*^{ash} model.

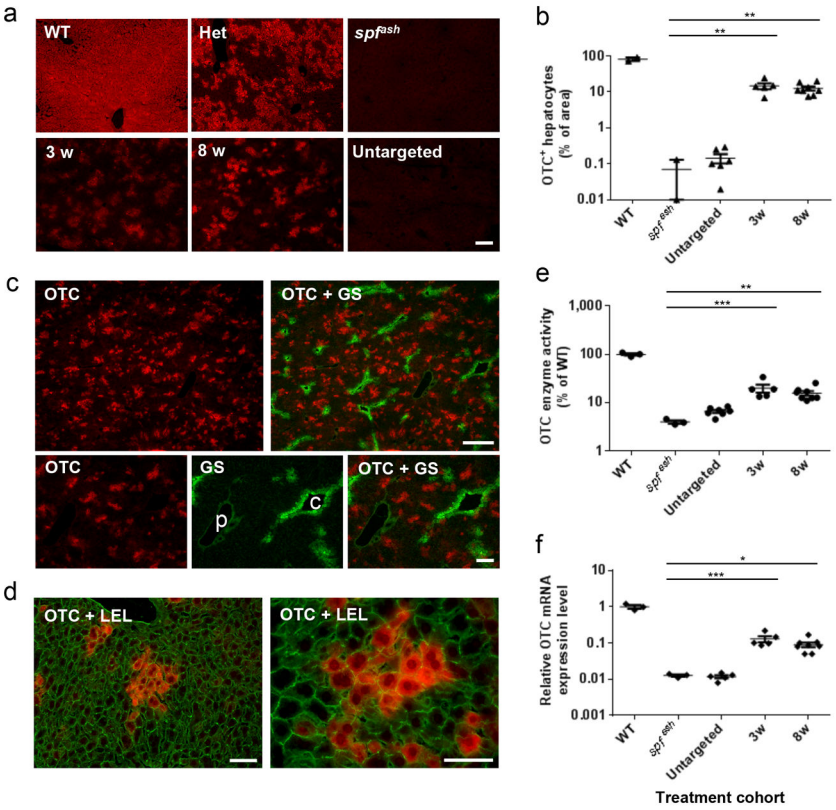

Figure 2. Efficient restoration of OTC expression in the liver of *spf*^{ash} mice treated at neonatal stage by AAV8.CRISPR-SaCas9-mediated gene correction

AAV8.SaCas9 (5×10^{10} GC/pup) and AAV8.sgRNA1.donor (5×10^{11} GC/pup) were administrated to postnatal day 2 (p2) *spf*^{ash} pups via the temporal vein. *spf*^{ash} mice were sacrificed at 3 (n=5) or 8 weeks (n=8) after treatment. Untargeted *spf*^{ash} mice received AAV8.SaCas9 (5×10^{10} GC/pup) and AAV8.control.donor (5×10^{11} GC/pup) at p2, and livers were harvested 8 weeks post treatment (n=6). Untreated WT (n=3) and *spf*^{ash} mice (n=3) were included as controls. (**a**) Immunofluorescence staining with antibodies against OTC on liver sections from *spf*^{ash} mice treated with the dual AAV vectors for CRISPR-SaCas9-mediated gene correction. Stained areas typically represent clusters of corrected hepatocytes. Untreated controls show livers from wild type, *spf*^{ash} heterozygous, and *spf*^{ash} hemizygous mice. Scale bar, 100μm. (**b**) Quantification of gene correction based on the percentage of area on liver sections expressing OTC by immunostaining as presented in panel a. (**c**) Random distribution of clusters of corrected hepatocytes along the portal-central axis shown by double immunostaining against OTC (red) and glutamine synthetase (GS, green), which is a marker of central veins (p, portal vein; c, central vein). Scale bars, 300 μm (upper panel) and 100 μm (lower panel). (**d**) Groups of corrected hepatocytes expressing OTC (red) shown by immunofluorescence on sections co-stained with fluorescein-labeled tomato lectin (Lycopersicon esculentum lectin, LEL; green) which outlines individual hepatocytes. Scale bar, 50μm. (**e**) OTC enzyme activity in the liver lysate of *spf*^{ash} mice at 3 and 8 weeks following dual vector treatment. (**f**) Quantification of OTC mRNA levels in the liver by RT-qPCR using primers spanning exons 4–5 to amplify wild-type *OTC*. Mean ± SEM are shown. * $P < 0.05$, ** $P < 0.01$, *** $P < 0.001$, Dunnett's test.

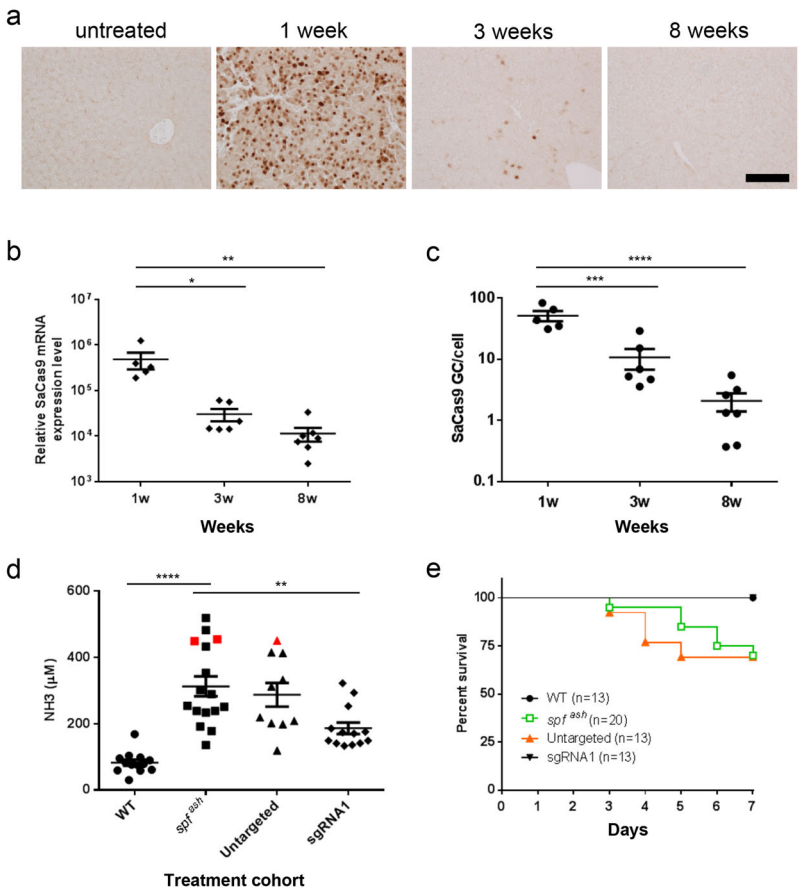

Figure 3. Time course of SaCas9 expression following neonatal vector administration and functional improvement following high-protein diet challenge

(a) Immunostaining with antibodies against FLAG on liver sections from an untreated mouse or treated *spf*^{ash} mice at 1, 3, or 8 weeks following neonatal injection of the dual AAV vectors for CRISPR-SaCas9-mediated gene correction. AAV8.SaCas9 (5×10^{10} GC/pup) and AAV8.sgRNA1.donor (5×10^{11} GC/pup) were administrated to p2 *spf*^{ash} pups via the temporal vein. Nuclear staining of FLAG-tagged SaCas9 were abundant at 1 week (n=5) but dramatically reduced at 3 weeks (n=6) and became scarce at 8 weeks (n=7) after vector injection. Scale bar, 100 μm. (**b**) Quantification of SaCas9 mRNA levels in liver by RT-qPCR. Mean ± SEM are shown. * $P < 0.05$, ** $P < 0.01$, *** $P < 0.001$, **** $P < 0.0001$, Dunnett's test. (**c**) Quantification of SaCas9 vector genome in liver by qPCR. (**d, e**) Plasma ammonia levels and survival curves in control or dual AAV vector-treated *spf*^{ash} mice after a one-week course of high-protein diet. Seven weeks following neonatal treatment with the dual AAV vectors, mice were given high-protein diet for 7 days. **(d)** Plasma ammonia levels were measured 7 days after the high-protein diet. Plasma ammonia levels in WT mice (n=13) and AAV8.SaCas9 + AAV8.sgRNA1.donor-treated *spf*^{ash} mice (n=13) were significantly lower than untreated *spf*^{ash} mice (n=16) after a 7-day high-protein diet. Red squares indicate samples obtained from moribund untreated *spf*^{ash} mice 6 days after high-protein diet; red triangle indicates sample obtained from a moribund *spf*^{ash} mouse treated with untargeted vector (AAV8.control.donor with no sgRNA1, n=10) 5 days after high-protein diet. ** $P< 0.01$, **** $P< 0.0001$, Dunnett's test. **(e)** Untreated *spf*^{ash} mice (n=20) or

spf^{ash} mice treated with untargeted vectors (AAV8.control.donor, n=13) started to die 3 days after high-protein diet. All WT (n=13) and AAV8.SaCas9 + AAV8.sgRNA1.donor-treated mice (n=13) survived. * $P < 0.05$, Mantel-Cox test.

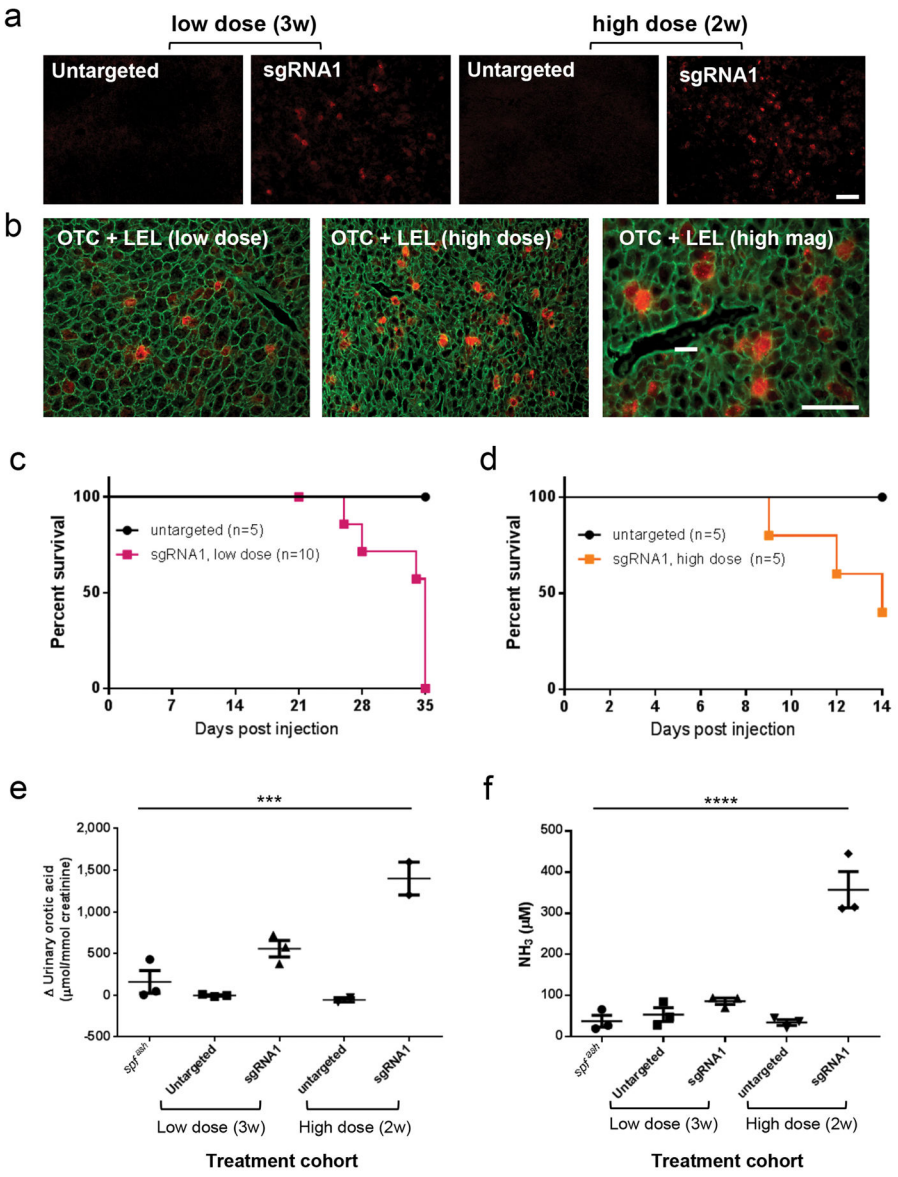

Figure 4. Gene targeting/correction in the liver of *spf*^{ash} mice treated as adults by AAV8.CRISPR-SaCas9 vectors

Adult *spf*^{ash} mice (8–10 weeks old) received an intravenous injection of AAV8.SaCas9 (1×10^{11} GC) and AAV8.sgRNA1.donor (1×10^{12} GC), or higher dose of AAV8.SaCas9 (1×10^{12} GC) and AAV8.sgRNA1.donor (5×10^{12} GC), or untargeted vectors at the equivalent doses. (**a**) Immunofluorescence staining with antibodies against OTC on liver sections collected at 3 (low-dose, n=3) or 2 weeks (high-dose, n=3) after injection. Stained cells typically showed as single corrected hepatocytes. Scale bar, 100μm. (**b**) Isolated corrected hepatocytes expressing OTC (red) shown by immunofluorescence on sections co-stained with fluorescein-labeled tomato lectin (LEL; green) which outlines individual hepatocytes. Scale bar, 50μm. (**c**) Survival curve of the low-dose cohorts: sgRNA1 (n=10) or untargeted vector at the same dose (n=5). (**d**) Survival curve of the high-dose cohorts: sgRNA1 (n=5) or untargeted vector at the same doses (n=5). The experiment was terminated at 14 days post

vector injection. (**e**) Change of urine orotic acid levels in adult *spf*^{ash} mice after treatment with high-dose gene targeting vectors (n=3 for untreated *spf*^{ash} and low-dose groups; n=2 for high-dose groups) (**f**) Elevation of plasma NH_3 levels in adult *spf*^{ash} mice after treatment with high-dose gene targeting vectors (n=3 for each group). Mean ± SEM are shown. *** $P < 0.001$, **** $P < 0.0001$, Dunnett's test.